lubricants

MDPI

Article

Improving the Surface Integrity and Tribological Behavior of a High-Temperature Friction Surface via the Synergy of Laser Cladding and Ultrasonic Burnishing

Nan Xu [1], Xiaochen Jiang [1,*], Xuehui Shen [1,*] and Hao Peng [2]

[1] School of Mechanical and Electrical Engineering, Shandong Jianzhu University, Jinan 250101, China; chenqu_sd@163.com
[2] School of Mechanical Engineering, Qilu University of Technology (Shandong Academy of Sciences), Jinan 250353, China; qilu_hao@163.com
* Correspondence: jiangxiaochen20@sdjzu.edu.cn (X.J.); xuehuishen@163.com (X.S.)

Abstract: Quite a lot of engineering friction components serve at high temperatures, and are thus required to have excellent friction and wear resistance. The said study aims to fabricate high-wear-resistance coating on ordinary low-cost materials, achieving the low-cost manufacturing of some high-end friction components that are usually made with expensive solid alloys. The coating was prepared via laser cladding with a sort of widely used Fe-based self-fluxing alloy powder. The chosen substrate material was forged 42CrMo, which is popular in high-temperature friction engineering applications. In order to achieve the best possible high-temperature friction and wear properties, the prepared coating was turned and then ultrasonic burnished. Three samples, i.e., the substrate sample, the cladded sample without burnishing, and the cladded sample with burnishing, were prepared. For the three samples, the surface characteristics and friction properties at a 200 °C temperature were compared and investigated. According to the results, the cladded sample with burnishing exhibited the best surface finishing and friction behavior. Ultrasonic burnishing after cladding led to a further hardness improvement of 15.24% when compared with the cladded sample without burnishing. Therefore, ultrasonic burnishing is an effective low-cost post-treatment method for a wearable coating serving at a high temperature.

Keywords: hybrid surfacing; wear resistance; additive manufacturing; surface modification

Citation: Xu, N.; Jiang, X.; Shen, X.; Peng, H. Improving the Surface Integrity and Tribological Behavior of a High-Temperature Friction Surface via the Synergy of Laser Cladding and Ultrasonic Burnishing. *Lubricants* **2023**, *11*, 379. https://doi.org/10.3390/lubricants11090379

Received: 8 August 2023
Revised: 3 September 2023
Accepted: 5 September 2023
Published: 7 September 2023

1. Introduction

42CrMo is widely used to manufacture engineering components owing to its excellent strength, toughness, and hardenability [1]. However, 42CrMo has low hardness and insufficient wear resistance [2,3]. Therefore, under high-temperature and pressure friction conditions, surface strengthening is necessary for this sort of material to meet some specific service requirements, for instance, a high wear resistance. Engine pistons, which serve at a max instantaneous temperature of about 2500 K, is a very typical case. In this case, the adhesion between friction pairs easily occurs.

Surface coating is a commonly applied surface modification method. There exists several coating preparation techniques for varying application cases, such as thermal spraying [4], electroplating [5], physical vapor deposition [6], etc. However, these techniques have varying defects including low coating and substrate bonding strength, a thin thickness, and environmental pollution [7]. Thus, these coating preparation methods are not very suitable in some cases similar to engine pistons.

Metal arc welding [8] and laser cladding [9] are two popular coating additive manufacturing techniques. Meanwhile, in recent years, laser cladding has been earning more engineering applications. Laser cladding utilizes an extremely high-energy-density laser beam to melt a layer of powder material on a substrate, and therefore, the cladding coating

is metallurgically bonded with the substrate. This technique can repair and remanufacture many high-end engineering parts with a much lower cost and less resource consumption [10]. Therefore, it has been earning more and more attention. Feng [11] prepared an Fe-based coating on a 42CrMo substrate via laser cladding and achieved apparent wear resistance improvement. Liu and Shi [12] used laser cladding to prepare a Ni-based self-lubricating coating on a 42CrMo substrate. They found that at a laser scanning speed of 300 mm/s, the sample obtained the least wear rate of 6.824×10^{-6} $mm^3/N{\cdot}m$ within the experimental scope. Kumar et al. fabricated a self-lubricating coating on a stainless steel substrate and achieved a 60% friction reduction at room temperature and a 40% friction reduction at 400 °C in comparison to the unmodified alloy [13].

However, in spite of their high bonding strength, cladding coatings still suffer from issues such as a rough surface finishing, tensile residual stress, and pores. These issues are mainly attributed to the difference of the thermal expansion coefficients between the cladding material and substrate as well as the rapid heating and cooling of the coating material. Therefore, in most cases, coatings need to be post-treated after cladding.

Ultrasonic burnishing (UB) is developed from traditional burnishing without ultrasonic vibration. This technique not only reduces the surface roughness, but also introduces compressive residual stress and refines the grain size, thus improving the mechanical properties of the treated materials [14]. Currently, ultrasonic burnishing technology is applied to various materials to improve different service performances [15]. Furthermore, the excellent process effect of UB has been established [16–18]. In terms of the post-treatment of cladding coatings, a few studies on UB could be found. For example, Hao [19] prepared an Inconel 625 multi-layer cladding coating on an H13 steel substrate. The coating was milled and then subjected to ultrasonic burnishing (UB). As a result, it was found that the treated coating had a surface roughness of less than 0.12 μm, and had better wear performance with less wear scars than the sample without UB. Ye et al. [20] applied ultrasonic burnishing on a laser-cladded Cr-Ni coating, and reported obvious fracture toughness improvement. Zhang et al. prepared Fe-based laser cladding coatings on carbon steel, and then treated the coatings via UB at room temperature and at a medium temperature of 200°, respectively. They reported a roughness decrease of 82.72% as well as a wear rate drop of 49.9% in comparison to the turned sample [21].

A few previous works have explored UB as a post-treatment of cladding coating. However, the effect of this technique crucially depends on the material [22]. Moreover, most available reports on the friction behaviors of cladding coatings were performed at room temperature, and investigations were rarely conducted at high temperatures. In this study, laser cladding and ultrasonic burnishing treatment was employed to address the shortcomings of 42CrMo friction surface serving at a high temperature, laying the foundation for meeting higher engineering requirements.

2. Experimental Details

2.1. Material and Sample Preparation

The substrate was a Ø50 × 30 mm forged 42CrMo bar. One end of the bar was turned to a roughness of Ra1.1μm and set as the cladding target surface. The composition of the substrate material was as follows: 0.43 wt % C, 0.31 wt % Si, 0.67 wt % Mn, 0.014 wt % P, 0.007 wt % S, 1.09 wt % Cr, and 0.20 wt % Mo and Fe margin. Before cladding, the substrate was cleaned in an ultrasonic acetone bath for 15 min.

The cladding material was a commercial Spherical Fe-based alloy powder with a grain diameter range of 10–30μm. The chemical composition was as follows: 0.43 wt % C, 0.31 wt % Si, 0.67 wt % Mn, 0.014 wt % P, 0.007 wt % S, 1.09 wt % Cr, and 0.20 wt % Mo and Fe margin. The left image in Figure 1 is the SEM photo of the chosen powder.

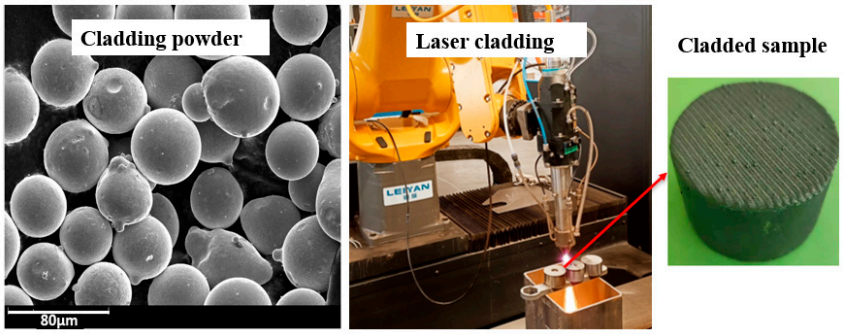

Figure 1. Cladding material and process.

Figure 1 shows photos of the laser cladding process and a cladded sample. The operation was performed on a robot laser cladding workstation (LYRF-4000) with an integrated control system (LYRF1500). The parameters of laser cladding were as follows: the laser power was 2000 W, spot diameter was 3.2 mm, scanning speed was 1500 mm/min, overlap rate was 30%, and powder feeding rate was 28.8 g/min. The distance of the spot from the surface being treated was about 15 mm. Argon served as protective gas with a flow rate of 5 L/min.

Self-developed ultrasonic burnishing equipment was used to post-treat the prepared cladding coatings. Tables 1 and 2 list the chosen parameters. Figure 2 shows the UB setup and illustrates the process principle. The detailed working principle of the designed UB device can be found in a previous work [23] and will not be further described here. After cladding, one sample was only hard turned (referred to as HT-treated sample), and the other was hard turned and then ultrasonic burnished (referred to as UB-treated sample). In addition, a forged 42CrMo sample was hard turned and set as the control.

Table 1. Turning parameters.

Cutting Depth (mm)	Spindle Speed (r/min)	Feed (r/mm)
0.1	300	0.06

Table 2. Ultrasonic burnishing parameters.

Frequency (kHz)	Amplitude (μm)	Feed (mm/min)	Static Load (N)	Spindle Speed (rpm)
28	7	10	320	160

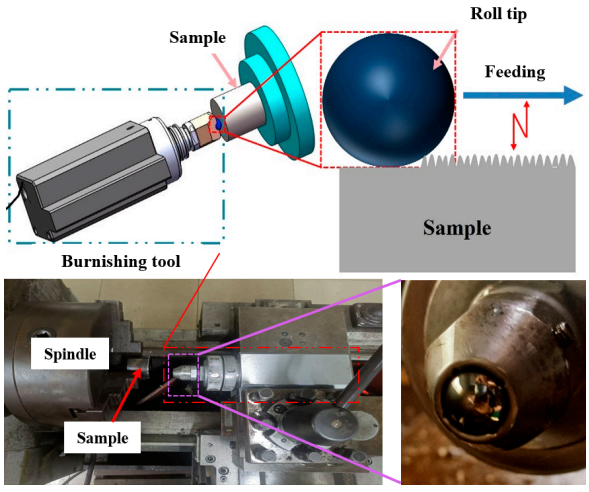

Figure 2. Schematic diagram and experimental setup of ultrasonic burnishing.

2.2. Microstructure Characterization

A scanning electron microscope (SEM, Phenom ProX, Eindhoven, the Netherlands) and its attached energy dispersion analyzer (EDS) were used to observe and measure the surface morphology and chemical composition of the samples. The sample surface morphology and roughness were observed and measured using a white light interferometer (Contour Elite K, Bruker Technology, Billerica, MA, USA). The samples were cut via WEDM and etched with aqua regia (a solution of HCl: HNO_3 = 3:1) to observe the microstructure. The sample microstructure was observed under a three-dimensional digital microscope (VHX-5000). XRD (D8-ADVANCE, Bruker, Germany) was used to determine the phase pattern. The chosen diffraction angle of the XRD was 20~85°, and the scanning speed was 5°/min. The samples were irradiated via Cu-kα ray (λ = 0.1542 nm) at 45 kV and 40 mA. Prior to XRD analysis, the samples were cleaned in an ultrasonic anhydrous ethanol bath for 10 min to remove surface impurities. The blind hole method was used to measure the surface residual stress. The porosity was calculated using ImageJ software from the SEM image. The microhardness was measured using a Vickers hardness tester (HXD-1000TMC). The section hardness was tested under a load of 500 GF and a holding time of 10 s. For each surface character parameter, five measurements were averaged to avoid random errors.

2.3. Wear

A ball-on-plate sliding wear experiment was conducted on a tribometer (HT-1000). The test temperature was set at 200 °C according to the usual working condition of piston pin-hole friction pair. The samples tested were shaped as blocks with dimensions of 20 mm × 10 mm × 5 mm as determined via WEDM. When being tested, the samples were slightly polished to remove oxides and then cleaned in an acetone bath for 10 min.

The counterbody was a Si_3N_4 ball with a 6 mm diameter and HV2200 hardness. The applied load was 150 N, and the mean and maximum contact pressures were 1.46 GPa and 2.19 GPa, respectively. The one-way sliding distance was 5 mm, the reciprocating frequency was 5 Hz, and the test holding time was 30 min. For each sample, three tests were performed to avoid gross error. The wear morphology was observed via SEM. Meanwhile, a white light interferometer and a 3D Super Depth Digital Microscope (VHX-5000) were used to measure the wear loss.

3. Results and Discussion

3.1. Surface Morphology and Porosity

Figure 3 shows the surface SEM images and the three-dimensional morphologies of the three prepared samples. In Figure 3a,b, for the control and HT-treated samples, there exists clear cutting marks with obvious peaks and valleys. In contrast, as shown in Figure 3c, the UB sample has a flat surface finishing without a visible cutting trace. According to the measurements, the roughness values of the three samples are Ra1.19, Ra1.12, and Ra0.17. Compared with the HT-treated sample, UB led to a 79.2% roughness reduction. The smoothing surface is a usual case for UB. During UB, the burnishing tool tip extruded the near-surface materials of the sample being treated to flow from peaks to valleys, and thus flattened the surface [24].

Another observation from Figure 3 is that, in all cases, there exists distributed black dots on the samples' surfaces. According to the EDS analysis, the content of the carbon element was relatively high at the black dots. It was analyzed that these black dots were pores and carbides generated in laser cladding. From Table 3, for the HT-treated and UB-treated samples, the contents of the major elements were not shown to be distinct except for carbon. UB smooths and strengthens the surface via material plastic deformation, and therefore, it could not cause a composition change in a usual case [23]. Here, for the UB-treated sample, the reduction in the C element was mainly attributed to the detachment of carbides [25]. Meanwhile, owing to the material flow from UB, some pores in near surfaces produced via laser cladding were filled [20], and thus, much fewer black dots were found in the UB-treated sample than in the HT-treated one.

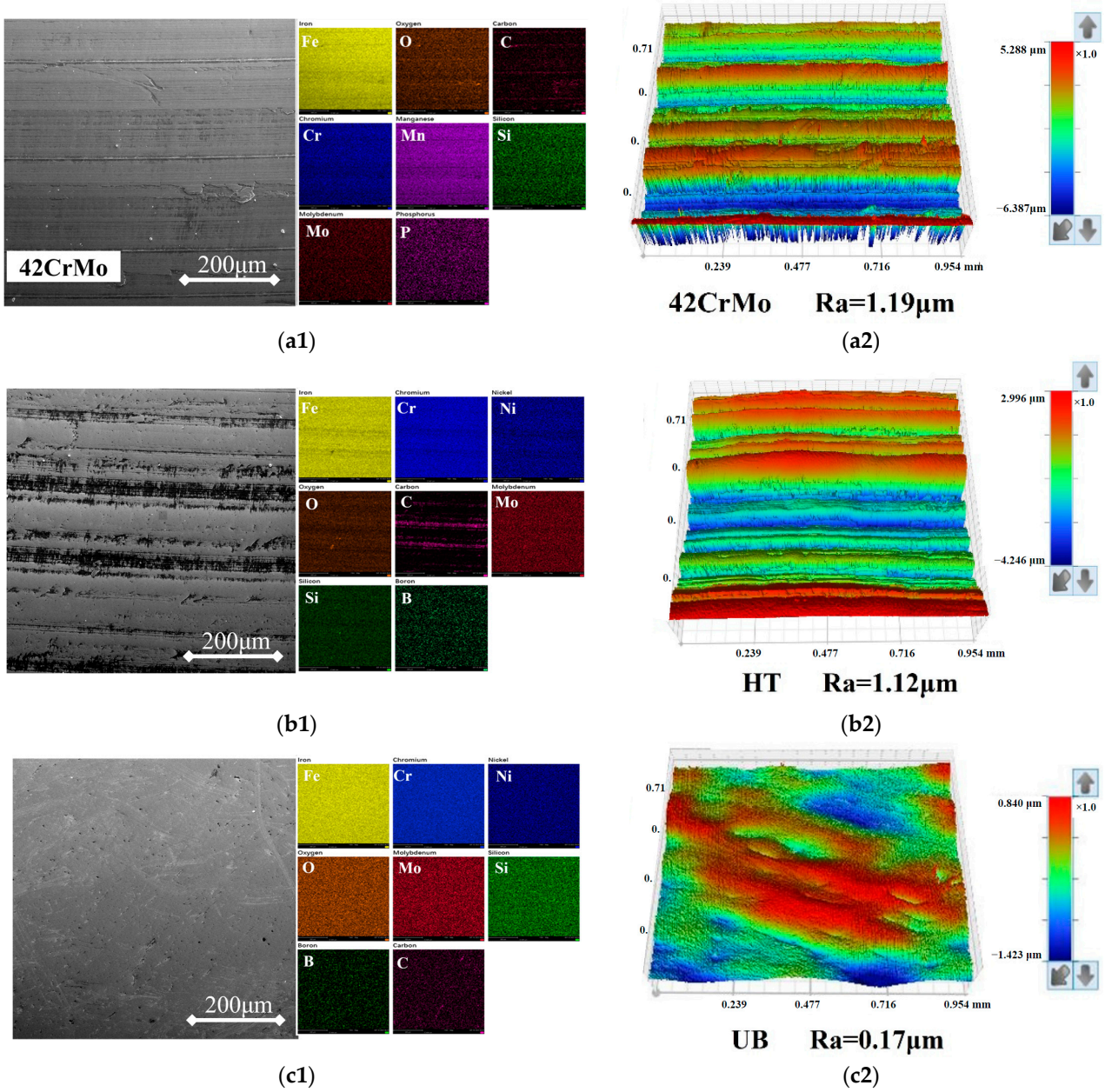

Figure 3. Surface SEM morphology. (**a1**) 42CrMo, (**b1**) HT samples, (**c1**) UB samples, and three-dimensional morphology: (**a2**) 42CrMo, (**b2**) HT samples, and (**c2**) UB samples. The EDS spectrum of UB samples is on the right side of (**a1**,**b1**,**c1**), respectively.

Table 3. Main element content of samples (wt%).

Samples	C	Si	Cr	Mo	Fe	Ni	O
Powder	0.43	0.31	1.09	0.20	97.28	-	-
Control	5.09	0.82	1.09	0.15	87.47	-	4.58
HT treated	11.89	1.59	14.41	1.18	49.88	5.44	12.23
UB treated	0.68	1.71	16.29	1.15	57.18	6.33	12.45

As shown in Figure 4, the porosity values of the control and HT-treated samples were 4.09% and 3.97%, respectively. The pores were generated from impurities and from gas generation during the melting and solidification of the powder. From Figure 4, turning alone could not improve the porosity inside the coating. In contrast, the UB treatment led to

an 85.6% porosity drop in comparison to the control. The significant pore elimination effect was attributed to the dynamic load from UB. In the experiment, the prepared cladding coat had a one-layer structure with about a 1 mm thickness. During UB, the applied high-frequency vibration could cause a dynamic stress wave propagating along an in-depth direction inside the coating [23]. Therefore, UB had a more strengthening effect than that of conventional burnishing without vibration.

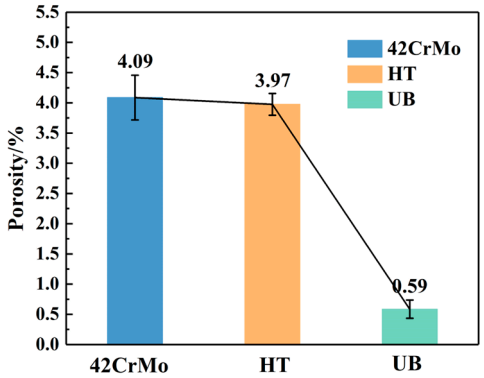

Figure 4. Porosity measurements.

3.2. Surface Microstructure

Figure 5 shows the surface microstructure of the samples with two magnifications, which were observed under a digital microscope after etching. From Figure 5(a1,a2), for the control sample, it can be seen that the 42CrMo material was mainly composed of tempered sorbite and ferrite. In Figure 5(b1,b2), there exists coarse strip-shaped and cellular dendrites. The shape of the dendrite structure is irregular and uneven. It is known that this sort of coarse microstructure is not conducive to mechanical performance. In contrast, from Figure 5(c1,c2), for the UB-treated sample, it can be seen that the dendrites were refined into equiaxed grains. Moreover, the sizes and shapes of the equiaxed crystals were uniform, making it easier to maintain a stable structure and thus have better mechanical properties. Grain refinement is a usual case in UB treatment, which is commonly explained as an outcome of dislocation slip, accumulation, interaction, annihilation, and rearrangement from the co-action of ultrasonic vibration and static load [26].

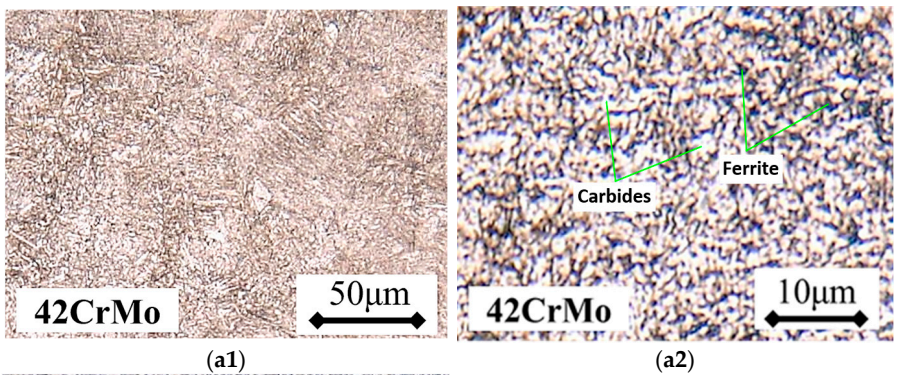

Figure 5. *Cont.*

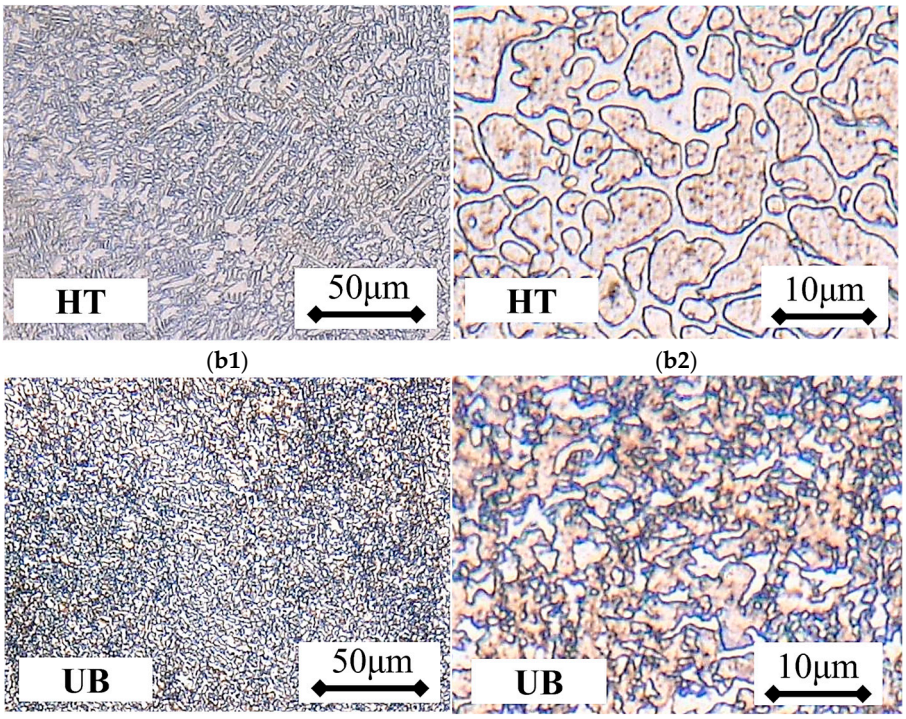

Figure 5. Surface microstructure: (**a1**,**a2**) control, (**b1**,**b2**) HT-treated, and (**c1**,**c2**) UB-treated samples.

3.3. XRD Analysis

The XRD pattern of the tree-tested samples are shown in Figure 6a. It can be observed that there was no clear element distribution variation for the HT-treated and UB-treated samples [25]. Figure 6a shows an enlarged view of the XRD's main peak. It can be seen that the peak intensity of the UB-treated sample was greatly weakened compared with the HT-treated one. This phenomenon was attributed to the grain reorientation, lattice distortion, and micro-strain resulting from UB [26]. Moreover, it is noted that the main peak of the XRD shifted to the right in the UB case, indicating an increase in the diffraction angle, a decrease in the crystal plane spacing, and an intensification of the micro-strain [27]. Figure 6b shows the FWHM measurements. Such values are 0.43 deg, 0.55 deg, and 0.74 deg, for the control, the HT-treated sample, and the UB-treated sample, respectively. According to the Scherrer equation, the broadening of the diffraction peak and the increase in the FWHM meant there was a decrease in the grain size [28,29], which agrees well with the microstructure above.

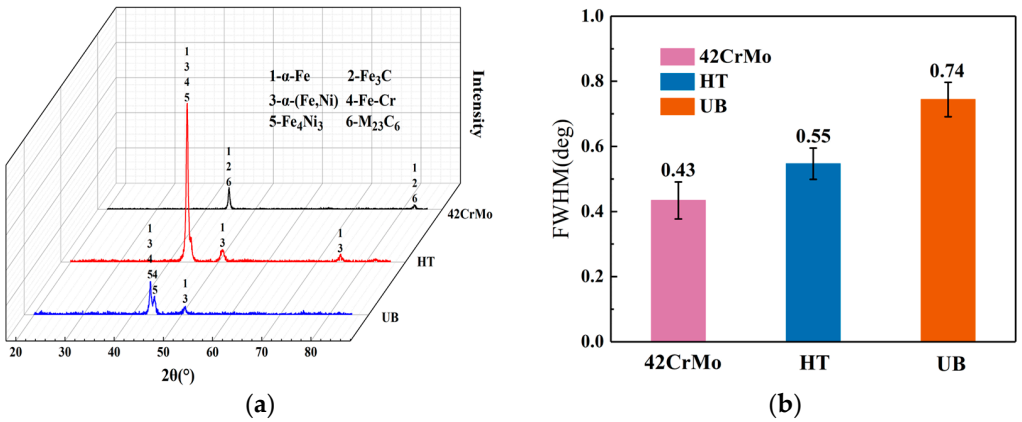

Figure 6. XRD measurements ((**a**) XRD spectrum; (**b**) FWHM measurements).

3.4. Residual Stress

Figure 7 shows the residual stress measurements. The residual stress values of the control and HT-treated samples are 404.48 ± 27.45 MPa and 571.48 ± 36.25 MPa, respectively, indicating tensile stress. Tensile residual stress introduction is the usual case for laser cladding. Two aspects are responsible for that. One is the great thermal expansion coefficient difference between the substrate and cladding material. The other is the rapid heating and cooling characteristics of the cladding process. It is known that tensile stress could facilitate crack initiation and propagation [30,31], and thus harm the mechanical property of the material.

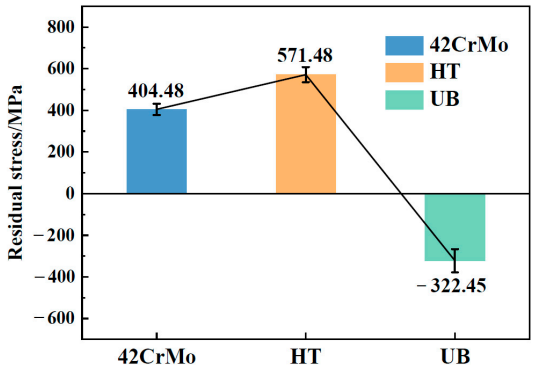

Figure 7. Residual stress measurements.

Compressive residual stress introduction is a key process effect of UB [32]. According to the results, the UB-treated coating had a compressive stress of about 322.45 MPa. Similarly, Korzynski et al. [33] also reported that ultrasonic burnishing could greatly improve the residual stress of the coating. The compressive stress introduction effect of UB could be explained from two aspects. On one hand, under the hammering of the burnishing tool tip, the near-surface materials flowed and deformed. Therefore, a layer of the near-surface material was compressed. On the other hand, UB introduced a large strain into the treated surface, generating high-density dislocations. The dislocation movement formed dislocation walls and entanglements, resulting in grain refinement [20,34]. Microstress was stored inside the refined grains, generating compressive stress. By combining Figures 6 and 7, it can be found that the residual stress measurements agree well with the diffraction peak shift.

3.5. Microhardness

The microhardness is the key to assess the wear behaviors of materials. As shown in Figure 8a, the surface microhardness values of the control and HT-treated coatings are 328.3 $HV_{0.5}$ and 416.6 $HV_{0.5}$, respectively. Compared with the control, the microhardness of HT-treated sample increased by 26.9%. The surface microhardness of the UB-treated sample was 480.1 $HV_{0.5}$, showing an increase of 15.24% compared to the HT-treated sample.

Figure 8b shows the varying in-depth hardness. The microhardness of the HT-treated sample was relatively stable in the coating region, while it sharply decreased at the coating–substrate interface. In contrast, the UB-treated sample exhibited a gradient hardness variation along the in-depth direction. During UB, the top surface material deformed the most, and the farther away it was from the top surface, the less deformation occurred [35,36]. Thus, UB could produce a gradient structure inside the coating, which was beneficial to the coating's wear resistance. Grain refinement was one main reason for the coating hardening. In the UB treatment, due to the material deformation, the crystal plane space and the distance between the atoms both decreased, and thus, the hardness was increased. In addition, the compressive residual stress introduction, the dislocation strengthening, and the work hardening were also responsible for the hardness improvement.

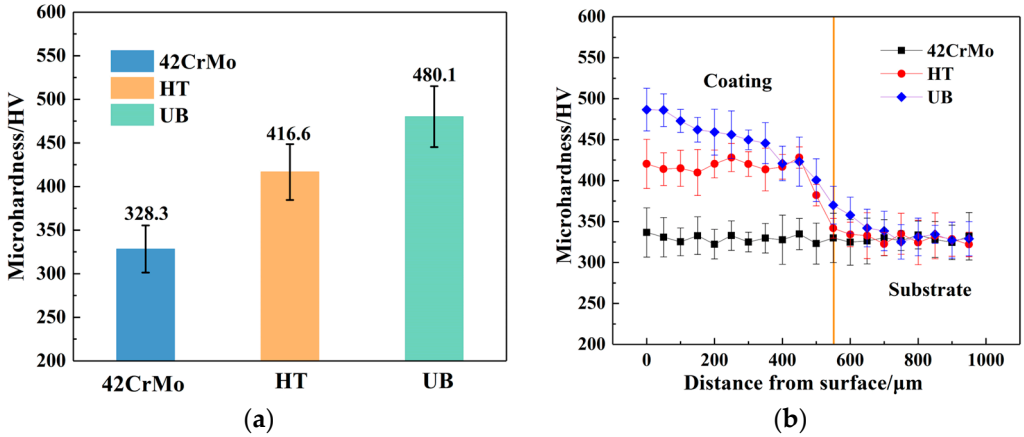

Figure 8. Microhardness measurements: (**a**) surface microhardness and (**b**) cross-sectional microhardness variation.

3.6. High-Temperature Friction Behavior

Figure 9a shows the friction coefficient varying for the three tested samples. The friction coefficient of all the samples increased rapidly at the beginning, and then decreased sharply, and finally became stable. Generally, the wear process includes three periods: running in, stable wear, and severe wear. Here, the running-in period was about 400 s. At this stage, the initial friction coefficients of the control and HT-treated samples were between 0.25 and 0.3, while such value for the UB-treated one was more than 0.4. Above all, according to the classic friction theory, it can be determined that all samples were in a boundary lubrication state. The larger friction coefficient of the UB-treated sample was mainly caused by lubricant loss from the smooth surface. In the control and HT-treated cases, there existed cutting marks, which could be served as lots of small lubricant reservoirs. In contrast, for the UB-treated sample, the smooth surface finishing facilitated lubricant loss.

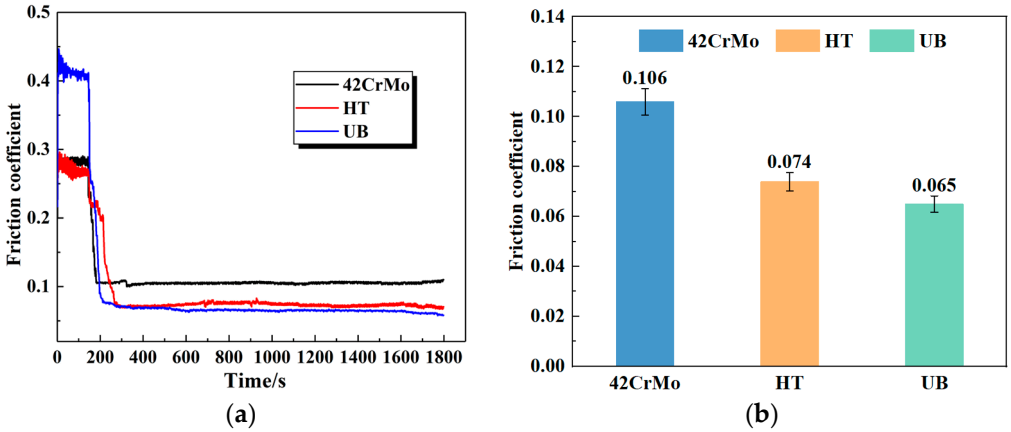

Figure 9. Friction coefficient measurements ((**a**) varying frictional coefficient; (**b**) average value).

At the stable wear period (400–1800 s), the contact area between the counterbody and the sample surfaces increased, and thus, the influence of the surface roughness greatly decreased. Meanwhile, a layer of oil film formed on the friction surface, which served to decrease the friction coefficient fluctuation. At this stage, the friction coefficient of the UB-treated sample was slightly lower than that of the HT-treated sample. The friction coefficient data in the stable friction period were averaged and are shown in Figure 9b. Compared to the value of the control sample, which was 0.106, the friction coefficient of the HT-treated sample decreased by 31.13%. Such value for the UB-treated sample was 0.065, which was further reduced by 10.96% compared to that of the HT-treated one. At this

stage, for all the three samples, the friction coefficients were in a range of 0.01–0.11, which indicated a hybrid of boundary lubrication and fluid lubrication. For the UB-treated sample, the decrease in the friction coefficient mainly resulted from surface improvement, including small roughness, high hardness, and the induced compressive residual stress [37,38].

Figure 10 shows the worn zone morphologies of the three samples. As shown in Figure 10a, in the control case, the sample surface suffered from severe wear along the sliding direction. There existed many debris, furrows, and pits, indicating abrasive and adhesion wear mechanism. At a high temperature, under the press load, the surface asperities slightly melted and welded with the counterbody instantaneously, and then with the sliding going on, peeling and cracks occurred.

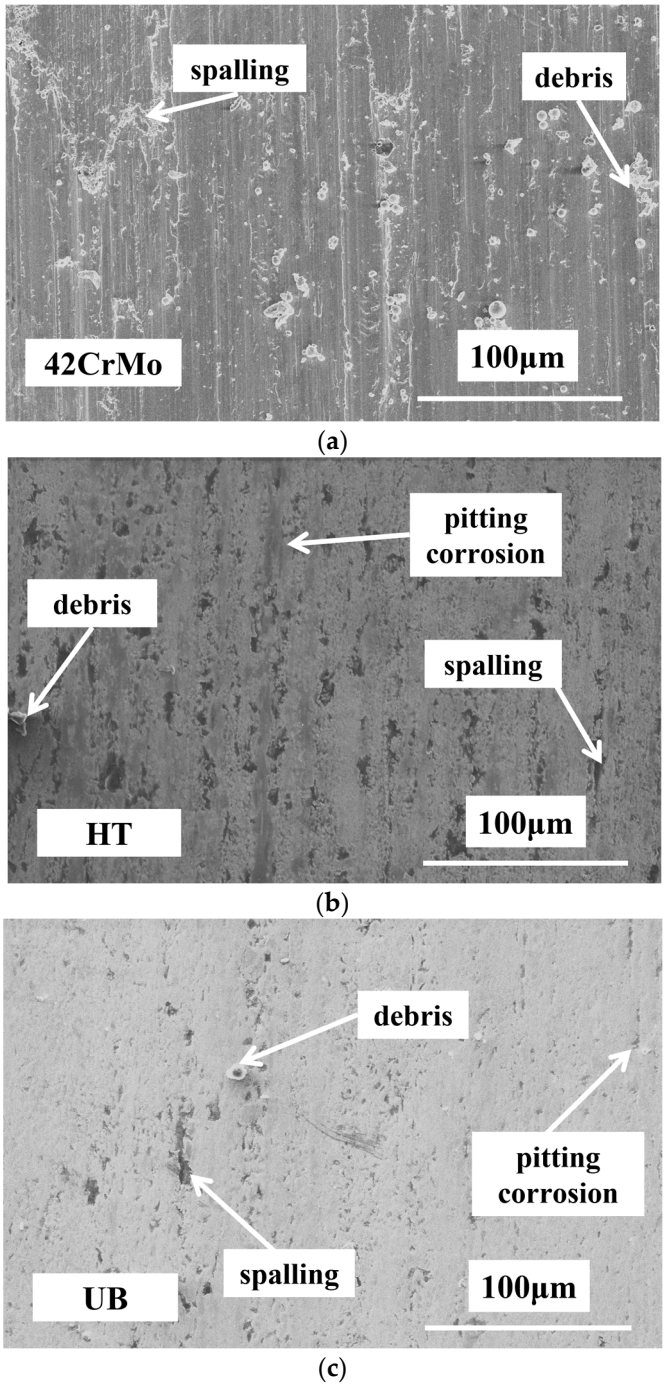

Figure 10. Worn zone images ((**a**) control; (**b**) HT-treated sample; (**c**) UB-treated sample).

In contrast, as seen in Figure 10b, the HT-treated surface had almost no plowing marks, and only a few wear debris were observed. However, there existed some pitting. As seen in Figure 10c, the worn morphologies of the HT-treated and UB-treated surfaces were similar. However, the latter had much less worn marks, exhibiting better wear resistance. The high hardness was mainly responsible for the wear resistance improvement.

The cross-sectional wear scar profiles of the three tested samples are shown in Figure 11a. Clearly, the control sample had the maximum worn depth and width, while the UB-treated one had the least worn dimension. The wear loss together with the wear rate were calculated and are compared in Figure 11b. The wear loss values of the control, HT-treated sample, and UB-treated sample were 0.071 mm^3, 0.024 mm^3, and 0.017 mm^3, respectively. In comparison to the control case, the wear rates of the two treated samples had a decrease of 66.62% and 76.06%, respectively. According to Archard's law, the wear loss is inversely proportional to the hardness. Here, the hardness and wear loss measurements conformed to the law.

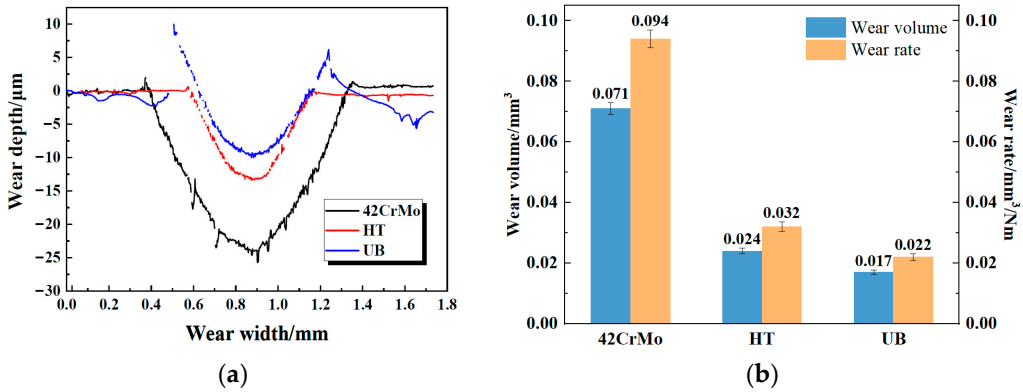

Figure 11. Worn zone measurements ((**a**) cross-sectional profile; (**b**) wear loss and wear rate).

The mechanism for the wear resistance improvement of the UB-treated surface could be explained from micro and macro aspects. At the micro level, as stated above, by UB, the grain was refined, and the amount and strength of the grain boundary both increased, making boundary slip difficult during sliding friction. At the macro level, UB caused work hardening and thus made the material difficult to deform. In addition, the compressive residual stress introduced from UB could serve to reduce the maximum shear stress and equivalent stress, and thus prevent surface crack initiation and propagation. Furthermore, the severe plastic deformation of the material from UB introduced high-density grain boundaries and dislocations, which could boost oxygen atom adsorption and thus form a dense oxide layer [39].

4. Conclusions

To improve the high-temperature wear resistance of some engineering parts, Fe-based alloy cladding coatings were prepared on a 42CrMo substrate via a laser and then post-treated via turning alone (HT-treated) or turning with an ultrasonic burnishing chain (UB-treated). The forged 42CrMo was set as the control for the comparative analysis.

The main conclusions are as follows:

(1) In comparison to the control, the hardness of the HT-treated sample was raised by 26.90%. However, turning alone could not improve the roughness or change the tensile residual stress.

(2) In comparison to the HT-treated sample, the UB-treated sample had a 79.2% roughness reduction, a further 15.2% increase in the hardness, and an 85.1% decrease in the porosity. Moreover, UB introduced compressive residual stress in the near-surface material of the coating.

(3) The two coated samples had better high-temperature wear resistance than the control. When compared with the HT-treated sample, although the UB-treated sample showed a larger friction coefficient in the running-in friction period, it had a lower friction coefficient and much less wear loss.
(4) A wearable coating serving at a high temperature could be manufactured and remanufactured via a laser and then post-treated via an HT-UB chain in a low-cost manner.

Author Contributions: Conceptualization, N.X. and X.S.; methodology, N.X. and X.S.; validation, N.X., H.P. and X.J.; investigation, X.J. and H.P.; writing—original draft preparation, N.X. and X.J.; writing—review and editing, N.X. and X.S. All authors have read and agreed to the published version of the manuscript.

Funding: This study was supported by the Shandong Provincial Natural Science Foundation (grant number ZR2023ME104).

Data Availability Statement: The data are contained within the article.

Conflicts of Interest: The authors declare no conflict of interest.

References

1. Qi, K.; Yang, Y.; Hu, G.; Lu, X.; Li, J. Thermal expansion control of composite coatings on 42CrMo by laser cladding. *Surf. Coat. Technol.* **2020**, *397*, 125983. [CrossRef]
2. Yang, Z.; Li, S.; Zhang, J.; Zhang, J.; Li, G.; Li, Z.; Hui, W.; Weng, Y. The fatigue behaviors of zero-inclusion and commercial 42CrMo steels in the super-long fatigue life regime. *Acta Mater.* **2004**, *52*, 5235–5241. [CrossRef]
3. Lin, Y.; Chen, M.; Zhong, J. Microstructural evolution in 42CrMo steel during compression at elevated temperatures. *Mater. Lett.* **2008**, *62*, 2132–2135. [CrossRef]
4. Tejero-Martin, D.; Rad, M.; McDonald, A.; Hussain, T. Beyond traditional coatings, a review on thermal sprayed functional and smart coatings. *J. Therm. Spray Technol.* **2018**, *28*, 598–644. [CrossRef]
5. Wu, H.; Wu, Y.; Yan, M.; Tu, B.; Li, Y. Microstructure and mechanical properties of surface coating prepared on grade 2 titanium by Ni-B composite electroplating and laser cladding. *Opt. Laser Technol.* **2023**, *164*, 109498. [CrossRef]
6. Jansons, E.; Lungevics, J.; Kanders, U.; Leitans, A.; Civcisa, G.; Linins, O.; Kundzins, K.; Boiko, I. Tribological and Mechanical Properties of the Nanostructured Superlattice Coatings with Respect to Surface Texture. *Lubricants* **2022**, *10*, 285. [CrossRef]
7. Xu, J.; Zhang, X.; Xuan, F.; Wang, Z.; Tu, S. Rolling contact fatigue behavior of laser cladded WC/Ni composite coating. *Surf. Coat. Technol.* **2014**, *239*, 7–15. [CrossRef]
8. Kołodziejczak, P.; Bober, M.; Chmielewski, T. Wear Resistance Comparison Research of High-Alloy Protective Coatings for Power Industry Prepared by Means of CMT Cladding. *Appl. Sci.* **2022**, *12*, 4568. [CrossRef]
9. Barr, C.; Rashid, R.; Palanisamy, S.; Watts, J.; Brandt, M. Examination of steel compatibility with additive manufacturing and repair via laser directed energy deposition. *J. Laser Appl.* **2023**, *35*, 022015. [CrossRef]
10. Rashid, R.; Nazari, K.; Barr, C.; Palanisamy, S.; Orchowski, N.; Matthews, N.; Dargusch, M. Effect of laser reheat post-treatment on the microstructural characteristics of laser-cladded ultra-high strength steel. *Surf. Coat. Technol.* **2019**, *372*, 93–102. [CrossRef]
11. Feng, Y.; Pang, X.; Feng, K.; Feng, Y.; Li, Z. Residual stress distribution and wear behavior in multi-pass laser cladded Fe-based coating reinforced by M 3 (C, B). *J. Mater. Res. Technol.* **2021**, *15*, 5597–5607. [CrossRef]
12. Liu, J.; Shi, Y. Microstructure and wear behavior of laser-cladded Ni-based coatings decorated by graphite particles. *Surf. Coat. Technol.* **2021**, *412*, 127044. [CrossRef]
13. Kumar, R.; Torres, H.; Aydinyan, S.; Antonov, M.; Varga, M.; Hussainova, I.; Ripoll, M. Tribological behavior of Ni-based self-lubricating claddings containing sulfide of nickel, copper, or bismuth at temperatures up to 600 °C. *Surf. Coat. Technol.* **2023**, *456*, 129270. [CrossRef]
14. Yin, M.; Cai, Z.; Zhang, Z.; Yue, W. Effect of ultrasonic surface rolling process on impact-sliding wear behavior of the 690 alloy. *Tribol. Int.* **2020**, *147*, 105600. [CrossRef]
15. Huang, H.; Wang, Z.; Lu, J.; Lu, K. Fatigue behaviors of AISI 316L stainless steel with a gradient nanostructured surface layer. *Acta Mater.* **2015**, *87*, 150–160. [CrossRef]
16. Zhao, J.; Liu, Z.; Wang, B.; Cai, Y.; Song, Q. Analytical Prediction and Experimental Investigation of Burnishing Force in Rotary Ultrasonic Roller Burnishing Titanium Alloy Ti-6Al-4V. *J. Manuf. Sci. Eng.* **2020**, *142*, 031004. [CrossRef]
17. Shi, Y.; Shen, X.; Xu, G.; Xu, C.; Wang, B.; Su, G. Surface integrity enhancement of austenitic stainless steel treated by ultrasonic burnishing with two burnishing tips. *Arch. Civ. Mech. Eng.* **2020**, *20*, 79. [CrossRef]
18. Teimouri, R.; Amini, S. Analytical modeling of ultrasonic burnishing process: Evaluation of active forces. *Measurement* **2019**, *131*, 654–663. [CrossRef]
19. Hao, J.; Hu, F.; Le, X.; Liu, H.; Han, J. Microstructure and high-temperature wear behaviour of Inconel 625 multi-layer cladding prepared on H13 mould steel by a hybrid additive manufacturing method. *J. Mater. Process. Technol.* **2020**, *291*, 117036. [CrossRef]

20. Ye, H.; Zhu, J.; Liu, Y.; Liu, W.; Wang, D. Microstructure and mechanical properties of laser cladded Cr-Ni alloy by hard turning (HT) and ultrasonic surface rolling (USR). *Surf. Coat. Technol.* **2020**, *393*, 125806. [CrossRef]
21. Zhang, C.; Shen, X.; Wang, J.; Wang, J.; Xu, C.; He, J.; Bai, X. Improving surface properties of Fe-based laser cladding coating deposited on a carbon steel by heat assisted ultrasonic burnishing. *J. Mater. Res. Technol.* **2021**, *12*, 100–116. [CrossRef]
22. Amanov, A. Effect of local treatment temperature of ultrasonic nanocrystalline surface modification on tribological behavior and corrosion resistance of stainless steel 316L produced by selective laser melting. *Surf. Coat. Technol.* **2020**, *398*, 126080. [CrossRef]
23. Shen, X.; Gong, X.; Zhang, J.; Su, G. An investigation of stress condition in vibration-assisted burnishing. *Int. J. Adv. Manuf. Technol.* **2019**, *105*, 1189–1207. [CrossRef]
24. Su, H.; Shen, X.; Xu, C.; He, J.; Su, G. Surface characteristics and corrosion behavior of TC11 titanium alloy strengthened by ultrasonic roller burnishing at room and medium temperature. *J. Mater. Res. Technol.* **2020**, *9*, 8172–8185. [CrossRef]
25. Gong, L.; Pan, Y.; Peng, C.; Fu, X.; Jiang, Z.; Jiang, S. Effect of ultrasonic surface rolling processing on wear properties of Cr12MoV steel. *Mater. Today Commun.* **2022**, *33*, 104762. [CrossRef]
26. Liu, D.; Liu, D.; Zhang, X.; Liu, C.; Ao, N. Surface nanocrystallization of 17-4 precipitation-hardening stainless steel subjected to ultrasonic surface rolling process. *Mater. Sci. Eng.-A Struct.* **2018**, *726*, 69–81. [CrossRef]
27. Su, Y.; Zhu, Y.; Zhang, B.; Zhou, H.; Li, J.; Wang, F. Spectral response of polarization properties of fiber Bragg grating under local pressure. *Opt. Fiber Technol.* **2015**, *25*, 15–19. [CrossRef]
28. Krzysztof, T.; Halina, G. Manufacturing of nanostructured titanium Grade2 using caliber rolling. *Mater. Sci. Eng. A Struct.* **2019**, *739*, 277–288.
29. Marcello, C. Minimum necessary strain to induce tangled dislocation to form cell and grain boundaries in a 6N-A1. *Mater. Sci. Eng. A Struct.* **2020**, *770*, 138420.
30. Suárez, A.; Amado, J.; Tobar, M.; Yanez, A.; Frag, E.; Peel, M. Study of residual stresses generated inside laser cladded plates using FEM and diffraction of synchrotron radiation. *Surf. Coat. Technol.* **2010**, *204*, 1983–1988. [CrossRef]
31. Shen, X.; He, X.; Gao, L.; Su, G.; Xu, H.; Xu, N. Study on crack behavior of laser cladding ceramic-metal composite coating with high content of WC. *Ceram. Int.* **2022**, *48*, 17460–17470. [CrossRef]
32. Ravil, K.; Young, S.; Pyun, C.; Min, S.; Riichi, M. Mechanical and fatigue characteristics of Ti-6Al-4V extra low interstitial and solution-treated and annealed alloys after ultrasonic nanocrystal surface modification treatment. *J. Nanosci. Nanotechnol.* **2014**, *14*, 9430–9435.
33. Korzynski, M.; Pacana, A.; Cwanek, J. Fatigue strength of chromium coated elements and possibility of its improvement with slide diamond burnishing. *Surf. Coat. Technol.* **2009**, *203*, 1670–1676. [CrossRef]
34. Ye, C.; Telang, A.; Gill, A.; Suslov, S.; Idell, Y.; Zweiacker, K.; Wiezorek, J.; Zhou, Z.; Qian, D.; Mannava, S.; et al. Gradient nanostructure and residual stresses induced by Ultrasonic Nano-crystal Surface Modification in 304 austenitic stainless steel for high strength and high ductility. *Mater. Sci. Eng. A Struct.* **2014**, *613*, 274–288. [CrossRef]
35. Fernandes, F.; Mahesh, K.; Silva, R.; Gurau, C.; Gurau, G. XRD study of the transformation characteristics of severely plastic deformed Ni-Ti SMAs. *Phys. Status Solidi C* **2010**, *7*, 1348–1350. [CrossRef]
36. Qin, W.; Li, J.; Liu, Y.; Yue, W.; Wang, C.; Mao, Q.; Li, Y. Effect of Rolling Strain on the Mechanical and Tribological Properties of 316 L Stainless Steel. *J. Tribol.* **2019**, *141*, 021606. [CrossRef]
37. Amanov, A.; Urmanov, B.; Amanov, T.; Pyun, Y. Strengthening of Ti-6Al-4V alloy by high temperature ultrasonic nanocrystal surface modification technique. *Mater. Lett.* **2017**, *196*, 198–201. [CrossRef]
38. Konyashin, I.; Ries, B.; Hlawatschek, D.; Zhuk, Y.; Park, D. Wear-resistance and hardness, Are they Directly related for nanostructured hard materials? *Int. J. Refract. Met. Hard* **2015**, *49*, 203–211. [CrossRef]
39. Amanov, A. Improvement in mechanical properties and fretting wear of Inconel 718 superalloy by ultrasonic nanocrystal surface modification. *Wear* **2020**, *446*, 203208. [CrossRef]